Inorganic Chemistry

Article

pubs.acs.org/IC

Labile or Stable: Can Homoleptic and Heteroleptic PyrPHOS–Copper Complexes Be Processed from Solution?

Daniel Volz,[†,§,¶] Manuela Wallesch,[†,‡,¶] Stephan L. Grage,[†,∥] Jörg Göttlicher,[⊥] Ralph Steininger,[⊥] David Batchelor,[‡] Tonya Vitova,[#] Anne S. Ulrich,[†,∥] Clemens Heske,[‡,⊥,▽,○] Lothar Weinhardt,*[,‡,⊥,▽] Thomas Baumann,*[,§] and Stefan Bräse*[,†,◆]

Institute of Organic Chemistry, Karlsruhe Institute of Technology (KIT), Fritz-Haber-Weg 6, 76131 Karlsruhe, Germany

Supporting Information

ABSTRACT: Luminescent Cu(I) complexes are interesting candidates as dopants in organic light-emitting diodes (OLEDs). However, open questions remain regarding the stability of such complexes in solution and therefore their suitability for solution processing. Since the emission behavior of Cu(I) emitters often drastically differs between bulk and thin film samples, it cannot be excluded that changes such as partial decomposition or formation of alternative emitting compounds upon processing are responsible. In this study, we present three particularly interesting candidates of the recently established copper–halide–(diphenylphosphino)pyridine derivatives (PyrPHOS) family that do not show such changes. We compare single crystals, amorphous bulk samples, and neat thin films in order to verify whether the material remains stable upon processing. Solid-state nuclear magnetic resonance (MAS ^{31}P NMR) was used to investigate the electronic environment of the phosphorus atoms, and X-ray absorption spectroscopy at the Cu K edge provides insight into the local electronic and geometrical environment of the copper(I) metal centers of the samples. Our results suggest that—unlike other copper(I) complexes—the copper–halide–PyrPHOS clusters are significantly more stable upon processing and retain their initial structure upon quick precipitation as well as thin film processing.

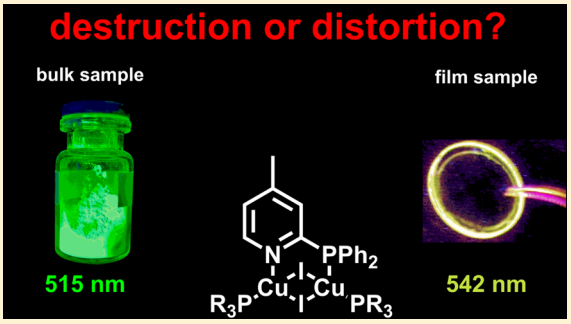

INTRODUCTION

Photoluminescent Cu(I) complexes[1−8] are increasingly employed as functional materials in optoelectronic devices such as organic light-emitting diodes (OLEDs),[9−13] light-emitting electrochemical cells,[14] oxygen sensors,[15] and—despite potential toxicity of Cu(I)—luminescent markers in biochemistry.[16,17] The use of copper has several advantages: Apart from the low price and good availability of various base materials, they have a favorable d^{10}-electron configuration, prohibiting many common quenching mechanisms involving empty, metal-centralized d orbitals.[5] Because of this, the photoluminescence quantum yield (PLQY) for Cu complexes can be very high, close to unity.[18,19] Most commonly, the copper moieties are directly involved in the luminescence because metal-to-ligand charge transfer (MLCT) emission occurs. This makes the emission spectrum easily tunable—a color spectrum ranging from blue to red has been covered with these compounds.[1−8] Many copper complexes feature a small singlet–triplet-splitting $\Delta E(S_1-T_1)$, which facilitates a thermally activated, delayed fluorescence[20,21] (TADF): This allows for a mixing of singlet and triplet states and a thermal repopulation of the excited S_1-state from the T_1-state at room temperature.[12,18,22,23] The result is a surprisingly short emission decay time (compared to phosphorescent materials) and a profound red shift upon cooling to 77 K.[22,24] Yersin et al. pointed out how this effect could lead to a theoretical quantum efficiency of 100% in OLEDs with Cu(I) compounds.[23] Such dopants are able to accept energy from both singlet and triplet excitons. Following the famous *triplet harvesting* concept[23,25] by Baldo, Thompson, and Forrest, this strategy is referred to as *singlet harvesting*.[10,22,23,26]

A potential drawback for Cu(I) compounds concerns their behavior upon device processing. Today, there are two competing strategies: vacuum evaporation and solution processing. While the first can be regarded as a standard procedure used in today's commercial OLED manufacturing, the second is mainly used in laboratory-scale OLED testing. Great effort is put into establishing reliable solution-processing techniques for this field[11,27−29] because they are expected to be faster and more cost- and material-efficient. Furthermore, only some of the Cu complexes are suitable for evaporation,[9,10] while many examples cannot be sublimated under standard conditions due to decomposition[30] or their ionic nature.[29] However, there is doubt regarding the stability of Cu(I) complexes in solution and therefore the applicability of solution processing for copper compounds: A profound red shift of several 10 nm is often noticed when making amorphous thin films.[31] This observation has been attributed to the effects of the rigidity of the surrounding matrix on the excited complexes.

Received: January 20, 2014
Published: July 16, 2014

   dx.doi.org/10.1021/ic500135m | *Inorg. Chem.* 2014, 53, 7837−7847

Scheme 1. Structures of the Studied Complexes

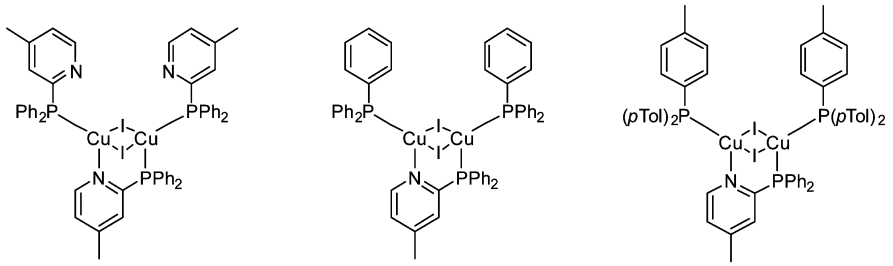

complex 1 homoleptic | **complex 2** heteroleptic | **complex 3** heteroleptic

For metal complexes featuring central metals such as iridium,[32,33] rhenium,[34−36] tungsten,[34] or ruthenium,[37−39] the effect is well-known: Due to rather long emission decay times (several microseconds) and therefore a greater thermal relaxation prior to emission, the matrix influences the geometry of the excited states and subsequently the exact emission color. However, regarding the solution chemistry of Cu(I), the applicability of this concept to copper complexes remains questionable. Generally, decomposition and, e.g., formation of other emissive species cannot be excluded. While the synthesis of complexes composed of Ir, Re, W, or Ru metal centers often needs higher temperatures to substitute ligands,[40] single-nuclear or multinuclear Cu(I) complexes can often be synthesized in one-pot reactions at low temperature by mixing ligands and Cu(I) sources, while the stoichiometry controls the products.[2,18,41,42] Common ligands are N,N-ligands (such as phenanthroline or neocuproine[43]), P, and P,P-ligands [such as bis(diphenylphosphino)diphenyl ether, POP[44]], or N,P-ligands [such as (diphenylphosphino)pyridine derivatives (PyrPHOS)].[45−47] Upon dissolving, equilibria of several species are often present in solution.[41,46,48−53] Schmittel and Ganz[54] and Pellegrin et al.[55] pointed out how heteroleptic Cu complexes with phenanthroline ligands form mixtures of homoleptic and heteroleptic compounds and how the equilibrium can be shifted toward the desired compounds by steric effects. In a recently published study by Nierengarten and co-workers,[56] dissociation equilibria in solution were systematically investigated for heteroleptic complexes of the type $[Cu(N,N)(P,P)]^+$. In this case, it was evidenced that the dynamic equilibria are mainly governed by the thermodynamic stability of the homoleptic $[Cu(N,N)]^+$ species and may be drastically changed by seemingly subtle alkyl substitutions near the coordination sites of the N,N-ligands. Even after isolation and in the solid state, some Cu(I) complexes undergo dissociation and rearrangement reactions. This has been shown for various examples of cationic PyrPHOS complexes featuring derivatives of PyrPHOS[57−61] as well as other P-donor ligands.[44,62−64]

Here, we try to shed some light on the question of whether the photophysical differences between bulk and thin film samples are a result of matrix rigidity or rather due to the formation of different emissive molecular species. Regarding the plethora of possible Cu(I) compounds, it is clear that a generalization of any result may be problematic. Because of their particular interest as dopants in OLEDs, three homoleptic and heteroleptic PyrPHOS complexes[8,18,19,45] were chosen to investigate if dissociation occurs upon film preparation. The photophysical properties of these known compounds are compared and amended by new data, while the local electronic structure around the phosphorus atoms and the local electronic and geometrical structure around the copper metal centers of amorphous and crystalline solids as well as thin film samples are probed with solid-state ^{31}P NMR and X-ray absorption spectroscopy (XAS) at the Cu K edge, respectively.

RESULTS

Structure and Photophysical Properties of Homoleptic and Heteroleptic PyrPHOS Complexes. The structures of all complexes investigated herein have been confirmed with single-crystal X-ray diffraction.[8,18,19] The basic molecular structure is given in Scheme 1, while some distances and angles are given in Table 3. We point out that, in principle, the terms homoleptic/heteroleptic do not apply here, because of the additional iodide ligands, making even complex **1** a heteroleptic compound. Since complexes similar to **1** have been named "homoleptic" repeatedly in the literature[8,18,19] and due to the lack of an alternative term to differentiate between complexes **1** and **2**/**3**, we chose to use them in the present way. All complexes contain a dimeric Cu_2I_2 unit, a bridging N,P-ligand, and two additional ligands that act as monodentate P-donors. In the case of the homoleptic complex **1**, two more equivalents of a PyrPHOS ligand fulfill this role, which leaves two potential N-donor positions uncoordinated. The heteroleptic complexes **2** and **3** contain two additional monodentate P-donors, triphenylphosphine and tris-*p*-tolylphosphine, respectively. It must be pointed out that—in principle—these structural models are only valid for single-crystal samples. For applications such as OLED manufacturing, these complexes are often rapidly precipitated as amorphous powders (for purification of bulk amounts of the compound) and processed into thin films by either evaporation or solution-processing protocols such as spin-coating, doctor-blading, or inkjet-printing. Regarding the published studies on copper complexes and their photophysical properties as amorphous powder, in solution, and as thin films, it is necessary to investigate whether the structure or even the stoichiometry of the complex is in agreement with the data obtained from single crystals. Using elemental analysis for carbon, nitrogen, and hydrogen, we confirmed that the empirical formula and composition of crystalline samples, amorphous powders, and thin films for complexes **1**−**3** are consistent within the accuracy of this method.

The frontier orbitals of complexes **1**−**3** have recently been calculated (Scheme 2).[8,19] All complexes show a similar behavior: the highest occupied molecular orbital (HOMO) is mainly located on the Cu_2I_2 unit, while the lowest unoccupied molecular orbital (LUMO) is located on the bidentate N,P-ligand, with most of the electron density on the pyridine

dx.doi.org/10.1021/ic500135m | Inorg. Chem. 2014, 53, 7837−7847

Scheme 2. Frontier Orbitals of Complex 1 Calculated with B3LYP (See Reference 8)[a,b]

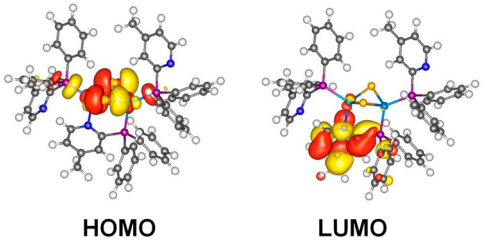

[a]The highest occupied molecular orbital (HOMO, left) is located on the Cu_2I_2 core, while the lowest unoccupied molecular orbital (LUMO, right) is located on the pyridine moiety of the bidentate MePyrPHOS ligand. The emissive transition has a strong (MX)LCT character. [b]Details regarding the DFT calculation of complex **1** have previously been published.[8] Scheme is adapted with permission from ref 8. Copyright 2013 American Chemical Society.

moiety. The HOMO−LUMO excitation thus has pronounced charge transfer character from the copper−iodide core to the bridging ligand. Time-dependent density functional theory (TDDFT) calculations with the BP86 functional show that the contribution of the HOMO−LUMO excitation to the lowest excited singlet state are >99% at the optimized ground-state structure.[8] So far it has been demonstrated that the emission color of PyrPHOS-type complexes can be modified by manipulation of the LUMO (different N,P-ligands) and the HOMO (different halides in Cu_2X_2).[18,65] One important difference between homoleptic complexes and their heteroleptic counterparts concerns their behavior in solution. It has been demonstrated that Cu(I) featuring N,P-ligands often show equilibria of several species when dissolved.[8,11,18,45,46,57] From a mechanistic point of view, a key step seems to be the breaking of a Cu−N bond and the subsequent formation of an intermediate 16-electron species. Due to the presence of noncoordinating pyridyl moieties in the homoleptic complexes, inter- as well as intramolecular rearrangement processes might occur.

The higher degree of dissociation for complex **1** is also reflected by the emission decay: While complexes **1**−**3** feature similar lifetimes in nondegassed solution (monoexponential decay with τ = 37, 45, and 39 ns, respectively), a removal of the quenching oxygen by degassing in Ar at room temperature for 45 min leads to lifetimes between 1.7 and 3.7 μs for complexes **2** and **3**, and a much shorter decay of 0.2 μs for complex **1** (Table 1).

Analysis of the decay rates k_r and k_{nr} (Table 2) reveals slower radiative and faster nonradiative rates for the homoleptic complex in solution, compared to the heteroleptic complexes. This difference vanishes in the solid state (powders as well as thin films): All three complexes feature relatively similar quantum efficiencies and emission decay times.

Comparing the emission spectra measured from different kinds of samples (powders, thin films, and solutions), several differences can be found (Figure 1): The film spectra feature a red shift relative to the powder spectra ($\Delta\lambda$ = 31, 31, and 11 nm, respectively, for complexes **1**−**3**), while the emission band is slightly broadened. In solution, this trend is continued with even broader bands and higher red shifts compared to the powder samples ($\Delta\lambda$ = 66, 62, and 42 nm for **1**−**3**). Earlier attempts to explain such behavior refer to a rigidochromic effect, first used to explain differences in emission spectra of

Table 1. Photophysical Properties of Complexes 1−3 for Powder, Solution, And Film[a]

		complex 1	complex 2	complex 3
powder	λ_{max}/nm	515	510	542
	PLQY **Φ**	0.89	0.99	0.74
	$\langle\tau\rangle$/μs	2.3	1.9	3.7
solution[b]	λ_{max}/nm	581	572	589
	PLQY **Φ**	0.02	0.24	0.14
	$\langle\tau\rangle$/μs	0.2	2.4	1.7
film[c]	λ_{max}/nm	546	541	553
	PLQY **Φ**	0.92	0.94	0.92
	$\langle\tau\rangle$/μs	3.7	2.3	2.2

[a]Some of the powder data were previously published elsewhere.[8,18,45]. λ_{max}. emission (peak maximum, excitation at 350 ± 1 nm); PLQY, excitation at 350 nm, with Φ error bar of ±0.02; $\langle\tau\rangle$ error bar, ±0.4 μs. Emission decay times were fitted using the intensity average lifetime as proposed by O'Connor and co-workers.[66] [b]Solutions were measured in degassed toluene at 10 mg mL^{-1} at room temperature. [c]Films were made by spin-coating from toluene onto quartz substrates; typical thickness was 20 nm.

Table 2. Analysis of Radiative and Nonradiative Decay Rates of Powder, Solution, and Film Samples of Complexes 1−3

	rate[a]/(10^6 s)	complex 1	complex 2	complex 3
powder	k_r	0.39	0.52	0.20
	k_{nr}	0.04	0.0062	0.07
solution[b]	k_r	0.01	0.10	0.08
	k_{nr}	4.99	0.32	0.51
film[c]	k_r	0.25	0.40	0.42
	k_{nr}	0.02	0.03	0.03

[a]Rates were calculated using the standard equations: see Supporting Information (SI) for details. [b]Solutions were measured in degassed toluene at 10 mg mL^{-1} at room temperature. [c]Films were made by spin-coating from toluene onto quartz substrates; typical thickness was 20 nm.

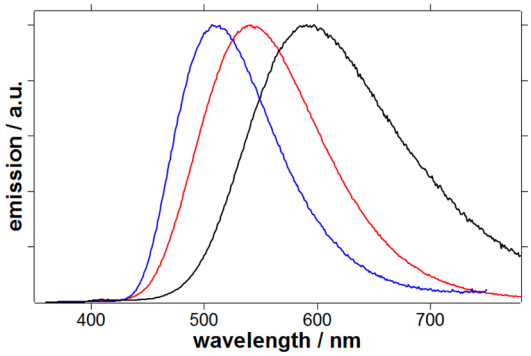

Figure 1. Emission spectra of complex **2**: from left to right, as a powder (blue), as a neat thin film (red), and in solution (black). Excitation at 350 nm.

Cu(I) clusters between solid and dissolved samples.[67] The observation that differences are also found when comparing thin films with bulk material raises the questions of whether this particular red shift is really a result of morphological effects such as the rigidity or electronic structure of the environment of the excited chromophores or whether other effects such as the actual formation of other species must be considered. We chose ^{31}P MAS NMR and X-ray absorption spectroscopy at the Cu K edge to analyze the molecular structures of the complexes in the solid state to answer these questions.

dx.doi.org/10.1021/ic500135m | Inorg. Chem. 2014, 53, 7837−7847

Solid-State ^{31}P NMR CP/MAS Experiments. Solid-state ^{31}P NMR was used to compare the structures of the copper complexes in the various solid morphologies studied because of its high sensitivity. The method has been used in a wide range of applications from inorganic materials to biological membranes.[68] It has been shown that this method is also able to distinguish between two structural isomers of a Cu(I) complex in a crystalline matrix.[69,70] We acquired solid-state ^{31}P NMR CP/MAS [nuclear magnetic resonance (NMR) using cross-polarization (CP) and magic angle spinning (MAS)] spectra of complex **1** prepared as a microcrystalline powder (Figure 2a), as a ground-up neat film (Figure 2b), and as an amorphous powder (Figure 2e). Compounds **2** and **3** were measured in the neat film state (Figure 2c,d) and as amorphous powder (Figure 2f,g).

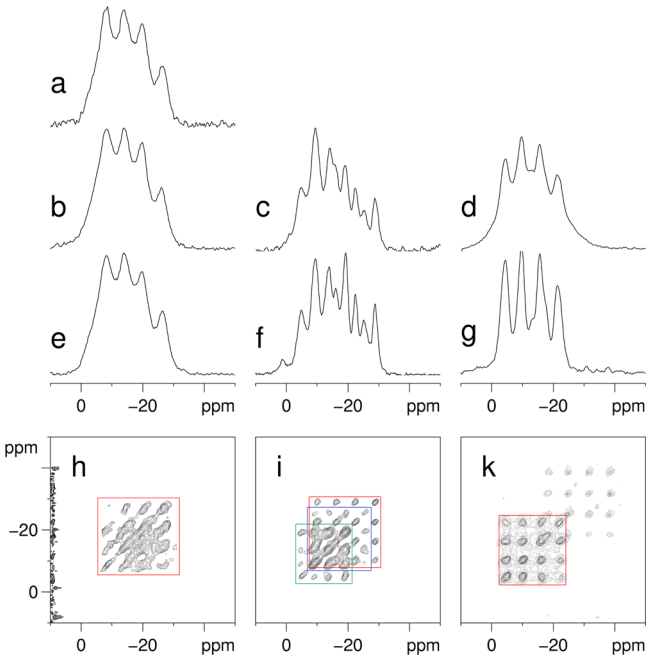

Figure 2. Solid-state CP/MAS ^{31}P NMR spectra (a–g) and two-dimensional ^{31}P–^{31}P correlation spectra (h–k) of the copper complexes **1** (a, b, e, h), **2** (c, f, i), and **3** (d, g, k), obtained at 242 MHz ^{31}P resonance frequency (600 MHz ^{1}H resonance frequency) under 25 kHz magic angle spinning and using cross-polarization from ^{1}H. We measured single crystals (a), thin films made by drop-casting (b–d), and amorphous powders (e–g). The spectra show one or several overlapping distorted quartets of the different ^{31}P sites, coupled to ^{63}Cu or ^{65}Cu. The two-dimensional ^{31}P–^{31}P correlation spectra (h–k) of the amorphous powder samples are shown below the corresponding one-dimensional spectra. The J-coupling networks are marked in color.

In solution, NMR peaks of complexes **1**–**3** are broad and ill-structured. As a consequence of the dynamic behavior mentioned in the previous section, ^{31}P NMR spectroscopy in $CDCl_3$ revealed only one P-component for the homoleptic complexes, despite the nonequivalence of the ligands.[8,11,46] The heteroleptic complexes feature at least two components, with one signal for the N,P-ligands and two broad, overlapping signals for the two P-donors.[19,45] In solid state, this situation is quite different: Complexes **1** and **3** are dominated by a quartet line shape, as expected from the J-coupling between ^{31}P and the spin 3/2 nucleus ^{63}Cu or ^{65}Cu. As reported in earlier studies on phosphorus/copper complexes, the peak positions and intensities of the quartet deviate from a regular symmetric multiplet due to incompletely averaged residual dipolar coupling as a consequence of the ^{63}Cu/^{65}Cu quadrupolar interaction and due the presence of the two isotopes of Cu.[69−72] The spectra of complex **2** (Figure 2c,f) are composed of several overlapping quartets. In order to discern the different contributions, two-dimensional (2D) ^{31}P–^{31}P correlation spectra were acquired for the amorphous powder samples of all complexes, which are shown below the corresponding one-dimensional spectra (Figure 2h–k). From the two-dimensional spectra, one, three, and two significantly differing J-coupling networks were identified for compounds **1**, **2**, and **3**, respectively. This corresponds to one, three, and two cross-peaks in the two-dimensional spectra. In the spectra of compound **3** as amorphous powder (Figure 2d,g), a second set of signals is visible upfield of the major quartet. This minor component also gives rise to a quartet, seen best in the two-dimensional spectrum (Figure 2k). We attribute these minor signals to a negligible fraction of less than ∼1% of trace impurities, while the major fraction (>∼99%) of complex **3** gives rise to a single quartet.

It is quite striking that complexes **1**–**3** seem to show a different number of ^{31}P resonances, despite their similar conformation. In principle, one would expect three separated signals, one for the bridging phosphine ligand and two more for the monodentate phosphines. However, none of the samples showed this behavior; instead, signals are obviously overlapping. This situation is quite similar to the results found in solution for PyrPHOS complexes,[11,18,19,45] where the use of monodentate arylphosphines led to one broad ^{31}P resonance in **1** and two ill-resolved signals in **2** and **3**, whereas the use of monodentate alkylphosphines led to two distinguishable signals (bridging aryl phosphine and monodentate alkylphosphine). In solid-state NMR, only complex **2** showed three readily identifiable signals, which would match the three different phosphorus atoms of the bridging and the two monodentate phosphines. The observation that complexes **1** and **3** possess overlapping quartets (indicated by the nonconcentric shape of the signals in the 2D plot) while several signals can be distinguished in complex **2** may be attributed to several effects, which are unlike the effects found in solution. The differences between the complexes in solid state probably reflect the impact of different substituents on the chemical environment, as well as differences in their molecular structures, with complex **2** deviating more from **1** and **3**. For example, as shown in Table 3, the Cu–Cu distance in **2** is increased and thus differs from those of complexes **1** and **3**. The angle between P–Cu–P for **2** is the largest among the three studied compounds. In solution, the broad, ill-structured signals may be related to an exchange of coordinated and dissociated ligands. Its sensitivity to small influences makes the solid-state ^{31}P NMR spectra a useful tool to probe for small structural differences.

Comparing the ^{31}P NMR spectra obtained by differently prepared samples, we notice that the peak positions are the same for the respective crystalline (Figure 2a) and amorphous powders (Figure 2b–d) or thin films (Figure 2e–g) of each complex. Hence the different processing does not seem to drastically change the local structure around the phosphorus atoms, suggesting that the local structure is indeed preserved during sample preparation.

However, a noticeable difference in the line width and relative intensities was observed for the different sample morphologies. Comparing the respective spectra of the neat

dx.doi.org/10.1021/ic500135m | Inorg. Chem. 2014, 53, 7837−7847

Table 3. Selected Bond Lengths and Angles for Complexes 1−3 (X-ray Diffraction)[a]

	complex 1	complex 2	complex 3
lengths			
Cu−Cu	2.753(1)	2.8164(5)	2.7135(7)
Cu_P−I	2.682(1)	2.6864(5)	2.6871(6)
	2.688(1)	2.6878(4)	2.6535(7)
Cu−-$P_{P,N}$	2.247(2)	2.2353(8)	2.250(1)
Cu−N	2.078(1)	2.090(2)	2.105(3)
Cu_N−P_P	2.253(1)	2.2533(7)	2.252(1)
Cu_P−P_P	2.247(1)	2.2493(7)	2.250(1)
angles			
Cu−I−Cu	62.34(1)	63.953(1)	60.837(2)
	61.85(1)	63.357(1)	61.213(2)
P−Cu−P	118.47(1)	123.90(3)	121.20(4)

[a]Bond lengths are given in angstroms; angles are in degrees.

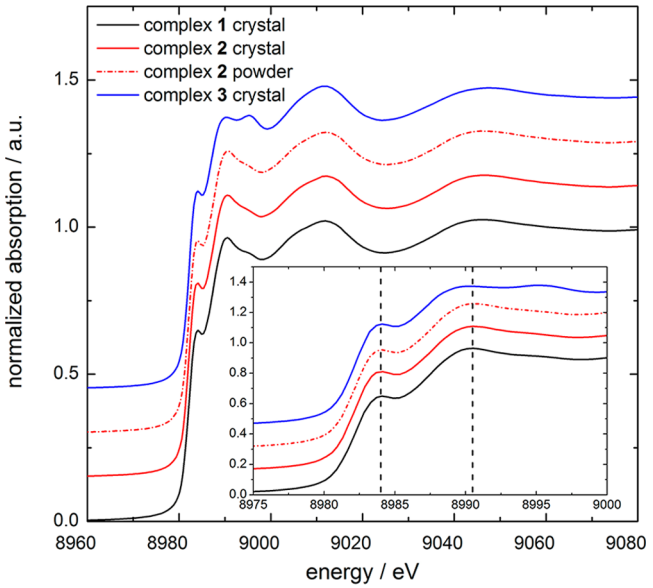

Figure 3. Cu K XANES spectra for crystalline samples of **1**, **2**, and **3** and a powder sample of **2**. Spectra are calibrated in energy (the inflection point of the edge of a Cu metal reference foil is set to 8980.3 eV[83]) and normalized to edge jump. The inset shows the edge region in more detail. Vertical line at 8984.0 and 8990.5 eV marks prominent features in the spectra.

film and amorphous powder of compounds **2** and **3**, the signals of the neat film spectra exhibit a larger broadening. In complex **1** this increase in line width is not observed; only the microcrystalline sample seems to possess slightly sharper lines than the other two morphologies of complex **1**. The origin of the differences in line width in complexes **2** and **3** could be either a different structural heterogeneity of the sample giving rise to dispersion in chemical shifts and couplings, a composition of microparticles of different size giving rise to different local susceptibilities, or different transverse relaxation times. The fact that the multiplets seem to be composed of lines with rather symmetric line shapes would favor relaxation to be the dominant cause of line broadening. It would also be conceivable that the bulk powder preparations possess a higher density and rigidity than the film preparations. The larger extent of slow molecular motions in the case of the film material would then lead to increased transverse relaxation and line width.

X-ray Absorption Spectroscopy in the XANES and EXAFS Region. Up to this point, we demonstrated that the composition of film and bulk samples is identical (elemental analysis), that there are no free ligands present, and that the chemical environment of the ligands, as defined by bonds, neighboring atoms, distances, and bond angles, does not change significantly (MAS NMR). In order to probe the local coordination geometry of the Cu(I) ions in the complex, we used X-ray absorption spectroscopy (XAS) at the Cu K edge in the XANES (X-ray absorption near-edge structure) and EXAFS (extended X-ray absorption fine structure) region. This is a well-established approach, e.g., to determine the coordination geometry of Cu-containing dendrimers,[73] metaloproteins,[74] or metastable complexes that cannot be crystallized.[9] This method has also been used to probe the excited-state geometry of various copper(I)−bisphenanthroline complexes in solution.[75−78] XAS has been used on copper complexes for almost 30 years[79] because of its high accuracy and sensitivity.[17,78,80,81] Information on the oxidation state as well as on the coordination number and symmetry of the copper ion can be extracted from the XANES region. XANES spectra for crystalline samples of complexes **1**, **2**, and **3** and a powder sample of complex **2** are depicted in Figure 3. Cu(I) complexes typically show low-energy peaks in the region between 8983.0 and 8986.0 eV and one peak at 8990.0 eV.[82] The former peaks are assigned as 1s → $4p_x$ and 1s → $4p_{y,z}$ transitions.[83] For the samples presented in this study these peaks were observed at 8984.0 and 8990.5 eV.

While complexes **1** and **2** do show a shoulder in the range between 8994.0 and 8997.0 eV in crystalline form, complex **3** exhibits another well-defined peak at 8995.3 eV. The XANES spectra of complex **2** in crystalline and amorphous powder form are very similar. In contrast, Cu(II) complexes show intense peaks in the region between 8986.0 and 8988.0 eV, which are assigned to 1s → 4p transitions, and exhibit a pre-edge peak at 8979.0 eV that corresponds to 1s → 3d transitions.[83] None of the copper−halide−PyrPHOS complexes presented in this study shows these features, which confirms that the d orbitals are fully occupied and that the oxidation state of copper is +1.[84] The energy position of the 1s → 4p transitions in Cu(I) complexes is correlated to the coordination number of Cu(I) and the symmetry of the ligand field around the central atom.[82,85] Ligand field theory predicts splitting of the degenerated $p_{x,y,z}$ orbitals of a Cu(I) ion in tetrahedral coordination upon distortion of the local geometry and changes to 3- and 2-fold coordination.[82,83] The energies of the 1s → 4p transitions (8984.0 and 8990.5 eV) are similar to the observed energies for other copper(I) iodide complexes and are in agreement with the distorted tetrahedral coordination of copper in these complexes.[9,86]

A comparison of the crystalline and film samples of complexes **1** and **2** is given in Figure 4. Single crystals from the same batch were also used to resolve the structure of complex **1** by single-crystal X-ray diffraction, so they serve as an additional reference with a known structure. We find that the primary features in the spectra of the crystalline form are all reproduced in the film spectra, which indicates that there is no drastic change in coordination geometry. However, for both complexes we find a "smearing out" of the first and second resonances and an additional feature around 8995.3 eV, as was also found in the spectrum of complex **3** in crystalline form. The origin of this feature requires further examination by

dx.doi.org/10.1021/ic500135m | Inorg. Chem. 2014, 53, 7837−7847

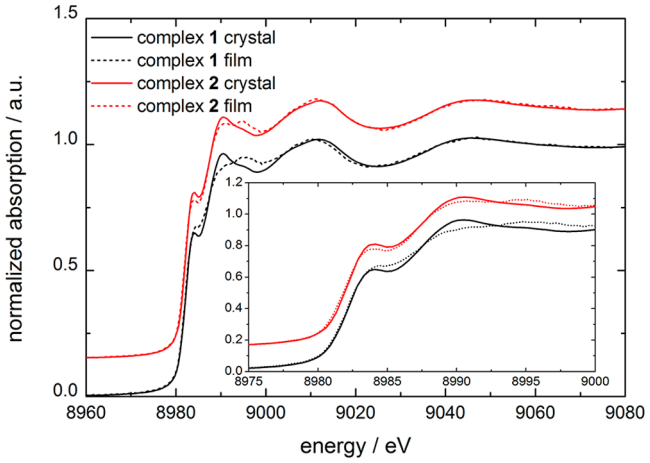

Figure 4. Cu K XANES spectra of complexes **1** and **2** in crystalline form and as thin film. Spectra are calibrated in energy and normalized to edge jump. The inset shows the edge region in more detail.

analyzing more samples and performing calculations of XANES spectra. A possible explanation may be a small change in the local geometry of the complex upon processing of thin films from solution. Further information on the local environment of the copper(I) centers can be drawn from the analysis of the EXAFS region (Figures 5 and 6). Whereas from the electronic

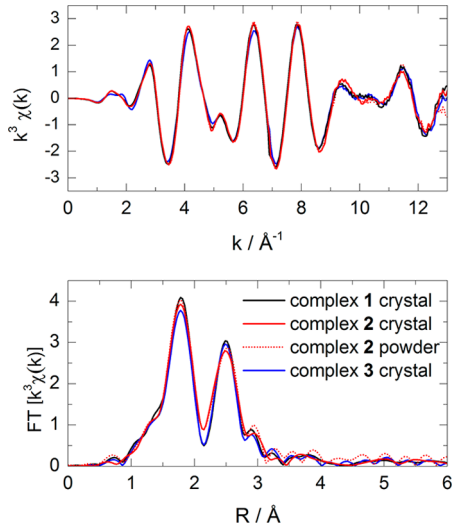

Figure 5. EXAFS data $k^3\chi(k)$ (top) and FT$[k^3\chi(k)]$ (bottom) of crystalline samples of complexes **1**−**3** and a powder sample of complex **2**.

structure reflected in the XANES spectra, information on the molecular geometric properties of the absorption site can be extracted, EXAFS can be used to derive nearest neighbor distances. Figure 5 presents EXAFS data in k space ($k^3\chi(k)$) for crystalline samples of complexes **1**−**3** and the powder sample of complex **2**, as well as the amplitude of the Fourier transformed $k^3\chi(k)$ (FT$[k^3\chi(k)]$) signal in R space. No significant differences are detectable between the EXAFS data of crystalline samples of complexes **1**−**3** and the amorphous powder sample of **2**, respectively. Furthermore, the EXAFS data of crystalline, amorphous, and film samples of complexes **1** and **2** are in good agreement with each other. The comparison of

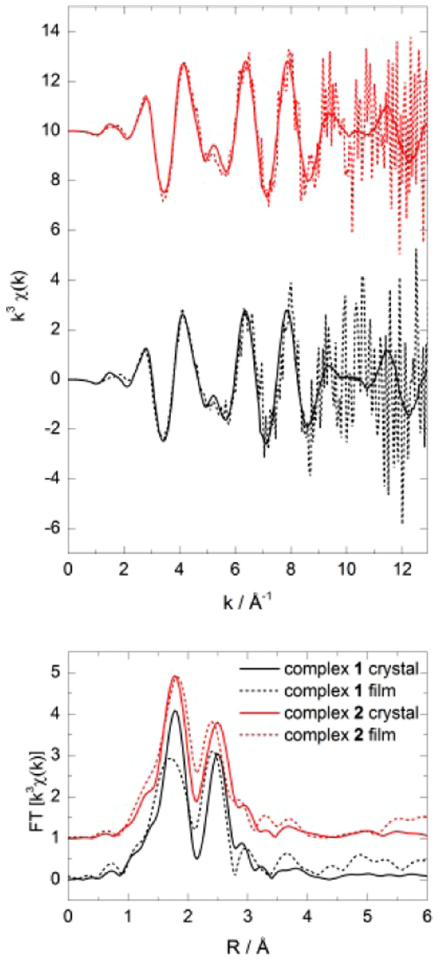

Figure 6. Comparison of EXAFS data $k^3\chi(k)$ (top) and FT$[k^3\chi(k)]$ (bottom) of a crystalline and a thin film sample of complexes **1** and **2**.

EXAFS data $k^3\chi(k)$ and FT$[k^3\chi(k)]$ of a crystalline and a thin film sample of complexes **1** and **2** are shown in Figure 6.

Interatomic distances and coordination numbers (Cu−N, Cu−P, Cu−I, and Cu−Cu) derived from the single-crystal X-ray diffraction analysis of the corresponding crystalline samples were used to set up the starting structures. One Cu−N, Cu−P, Cu−I, and Cu−Cu single scattering path was included to obtain the best fits. As an example the best fits for a crystalline and a film sample of complex **1** are shown in Figure 7. The obtained structural data are collected in Table 4. For all samples, the coordination numbers are in reasonable agreement with the mean coordination numbers (N) of the two copper centers derived from the crystal structure (N(N) = 0.5, N(P) = 1.5, N(I) = 2.0, and N(Cu) = 1.0), given the high correlation between coordination numbers and Debye−Waller factors in particular in view of the rather high Debye−Waller factors found for the Cu−Cu path. The interatomic distances Cu−N and Cu−P are in good agreement, whereas the Cu−I distances are about 0.1 Å shorter and the Cu−Cu distances are about 0.2 Å longer obtained from EXAFS compared to single-crystal diffraction results. Such differences are possible due to the sensitivity of the EXAFS spectrum to the mean short-range atomic order around the absorbing atom, whereas long-range order is measured in single-crystal diffraction.

The peak between 1.0 and 2.1 Å (not phase-shift-corrected) is modeled with Cu−N, Cu−P, and Cu−I scattering paths. The peak between 2.1 and 3.4 Å (not phase-shift-corrected)

dx.doi.org/10.1021/ic500135m | Inorg. Chem. 2014, 53, 7837−7847

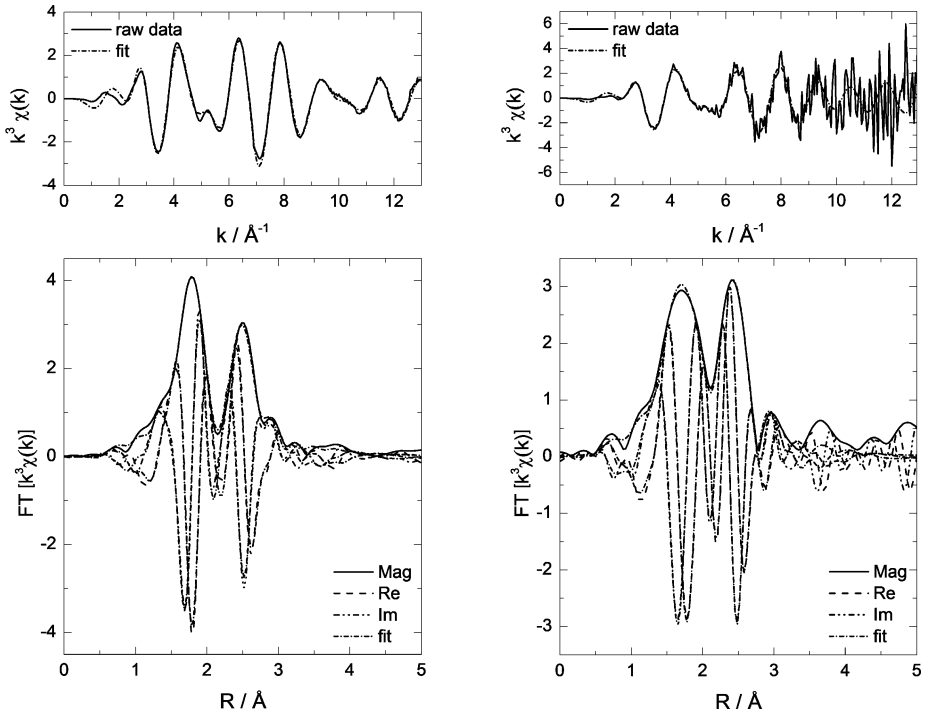

Figure 7. EXAFS data $k^3\chi(k)$ (top) and FT$[k^3\chi(k)]$: magnitude (Mag), real (Re), and imaginary (Im) parts (bottom) and their best fits for a crystalline (left) (FT range k = 2.3−12.2 Å^{-1}) and a thin-film sample (right) (FT range k = 2.3−11.2 Å^{-1}) of complex **1**.

Table 4. EXAFS Results for Crystalline and Film Samples of Complex 1[a]

path	R/Å	N	ΔR/Å	σ^2/Å^2
Complex 1 (Crystalline), R-Factor = 0.002				
Cu−N	2.10	0.6 ± 0.1	0.01 ± 0.01	0.006 ± 0.000
Cu−P	2.25	1.1 ± 0.1	0.01 ± 0.01	0.006 ± 0.000
Cu−I	2.64	1.4 ± 0.1	−0.05 ± 0.01	0.011 ± 0.001
Cu−Cu	3.05	1.6	0.23 ± 0.02	0.021 ± 0.003
Complex 1 (Film), R-Factor = 0.001				
Cu−N	2.10	0.9 ± 0.2	−0.01 ± 0.01	0.008 ± 0.001
Cu−P	2.25	1.1 ± 0.2	−0.01 ± 0.01	0.008 ± 0.001
Cu−I	2.64	1.2 ± 0.1	−0.09 ± 0.01	0.008 ± 0.001
Cu−Cu	3.05	1.8	0.27 ± 0.04	0.026 ± 0.006

[a]From left to right: single scattering paths used in the fit (path), interatomic distances (R), coordination numbers (N), deviation from the distances obtained from the XRD analyses, and mean squared atomic displacement/Debye−Waller factors (σ^2). The N(Cu) is restrained during the fit N(I) + N(Cu) = 3.

describes the scattering of the photoelectron from I and Cu atoms (Cu−I and Cu−Cu). The Cu−I single scattering path has a complex shape and contributes in both peaks (see the Supporting Information (SI)). The amplitude reduction factor S_0^2 = 0.9, which accounts for multielectronic excitations, is obtained from a fit of an EXAFS spectrum of a metallic Cu foil measured in the same experimental conditions. S_0^2 is fixed to 0.9 for all fits. The values for the energy threshold offset ΔE_0 extracted from the fits are 0.6 ± 0.3 eV for the crystalline sample of complex **1** and −0.6 ± 0.4 eV for the thin-film sample of complex **1**.

The Debye−Waller factors σ^2 derived from the model fit lie between 0.005 and 0.026 Å^2, with increasing values corresponding to longer interatomic distances. The relatively high values for the Cu−Cu path not only can be attributed to thermal disorder at room temperature[81,87] but also suggest a static disorder contribution.[88] Comparing the fitting results for crystalline and film samples shows that there are no significant differences between the spectra as the results for ΔE_0, N, R, and σ^2 are very similar within the error bars. Combining XANES and EXAFS results with further evidence from elemental analysis and solid-state NMR leaves the structure where Cu is coordinated on average by 0.5 N, 1.5 P, 2.0 I, and 1.0 Cu atoms as the only chemically reasonable model structure.

In summary, the comparison of XANES and EXAFS spectra of crystalline and film samples indicates that the coordination geometry around the copper(I) center as well as the type and distance of nearest neighboring atoms is retained upon solution processing of the investigated copper complexes **1** and **2**. The aforementioned feature at 8995.3 eV in the XANES region in crystalline samples will be the subject of further investigations. We speculate that it may be caused by minor angular distortions of the Cu_2I_2 unit. Even when the Cu−I and Cu−Cu-distances are retained (as indicated by the EXAFS results), there remains a certain degree of freedom regarding the angles between the Cu−Cu−I_1 and Cu−Cu−I_2 planes. We can also confirm that amorphous samples of complex **3** feature the expected coordination geometry.

■ CONCLUDING DISCUSSION

Combining the XRD, NMR, EXAFS, and XANES results, we find strong evidence that the atomic arrangement within the probed molecules is comparable for single crystals and amorphous thin films of the three investigated compounds, since the NMR and EXAFS results for these samples are in good agreement with each other. This, in turn, suggests that the large color shift in combination with the preservation of the PLQY, the emission decay times, and the rates k_r and k_{nr} cannot be explained by dissociation of the complexes. The popular, well-established theory of rigidochromic effects on quantum efficiency assumes both color and efficiency are influenced by

dx.doi.org/10.1021/ic500135m | Inorg. Chem. 2014, 53, 7837−7847

matrix effects on the structure. This, however, does not seem to provide a sufficient explanation for our results. However, upon close examination, minor differences are apparent in the XANES region of the XAS spectra and the line width in the NMR. The line width effects found in MAS ^{31}P NMR suggest that the rigidity in bulk samples is indeed higher than in thin films. Surprisingly, this does not seem to influence the PLQY in our case. While the exact reason for this requires further investigation, one possible explanation could be a combination of rigidochromic effects with a distortion of the ground-state geometry of the complexes. This could also be the reason for the differences found in the XANES spectra of the complexes. In our case, the HOMO is located on the Cu_2I_2 unit of the complexes.[19] Changes in this unit, for example, by widening or flattening of the I−Cu−I angles, are thus likely to cause color shifts, while still being in accordance with all other spectroscopic results.

We conclude by answering the initial question: Our results suggest that homoleptic and heteroleptic PyrPHOS complexes are indeed stable enough to be processed from solution. We analyzed the situation in single crystals, amorphous powders, and thin films from the point of view of the metal center (EXAFS, Cu K edge) as well as the ligands (^{31}P NMR). All results indicate that—within the accuracy of our methods—this class of materials retains its principle structure even when preparing thin films by solution-processing methods. Both the chemical environment of the P atoms and the number, type, and distance of any ligands relative to the copper atoms are maintained. This suggests that the here-chosen complexes offer the opportunity to be used in optoeletronic device applications even when processed as thin films from solution.

■ EXPERIMENTAL SECTION

All complexes were synthesized according to the procedures given in the references.[8,19,45] The crystalline samples were made by growing single crystals from dichloromethane/ether. Amorphous powders were made by precipitation from dichloromethane in methanol. Neat film samples were obtained by spin-coating of concentrated solutions of the compounds on quartz glass substrates (1×1 cm^2) in air.

Photophysical Measurements. Emission and excitation spectra were measured with a Horiba Scientific FluoroMax-4 spectrofluorometer using a JX monochromator and a R928P PMT detector. Fluorescence lifetime measurements were recorded and detected on the same system using the time-correlated single photon counting (TCSPC) method with the FM-2013 accessory and a TCSPC hub from Horiba Jobin Yvon. For this, a NanoLED 370 was used as excitation source (λ = 370 nm, 1.5 ns pulse). Decay curves were analyzed with the software DAS-6 and DataStation provided by Horiba Jobin Yvon. The quality of the fit was determined by the χ^2 method of Pearson.[89]

For the determination of the photoluminescence quantum yield, Φ, an absolute PL quantum yield measurement system from Hamamatsu Photonics was used. The system consisted of a photonic multichannel analyzer PMA-12, a model C99200-02G calibrated integrating sphere, and a monochromatic light source L9799-02 (150 W Xe and Hg−Xe lamps). Data analysis was performed with the PLQY measurement software U6039-05, provided by Hamamatsu Photonics.

Solid-State NMR Measurements. Neat film samples were obtained by spin-coating of concentrated solutions of the compounds on glass substrates (3×5 cm^2), drying, and scraping off the material. The samples were ground to a fine powder and filled into 2.5 mm outer diameter rotors for solid-state ^{31}P NMR measurements using MAS. To rule out changes in the samples by this sample preparation, the ground powders were observed under UV light (366 nm) and compared to the nonmodified samples to confirm that the luminescence color did not change. All ^{31}P NMR experiments were performed at a resonance frequency of 242 MHz (corresponding to 600 MHz for ^{1}H) and 25 kHz sample spinning, using a wide-bore magnet and a Bruker Avance spectrometer (Bruker Biospin) equipped with a double-tuned MAS probe. The ^{31}P NMR spectra were acquired using ramped CP[90] from protons, with a contact time of 5 ms and a radiofrequency field strength of 50 kHz to avoid long recycle times due to the long longitudinal relaxation time of ^{31}P in the copper complexes. Two-dimensional ^{31}P−^{31}P correlation experiments were obtained using a spin exchange pulse sequence,[91] employing a mixing time of 200 ms and between 128 and 256 increments of ∼40−80 μs dwell time each. The signal was acquired for 16−32 ms under 80 kHz proton decoupling. Typically 512 scans for the one-dimensional and 16−64 scans for the two-dimensional spectra were averaged, with a recycle delay of 3 or 10 s in the one-dimensional spectra of complex **3**. All spectra were processed using the Topspin software and applying a line broadening of 100 Hz.

X-ray Absorption Spectroscopy (XANES, EXAFS): Sample Preparation and Measurements. Crystalline and powder samples were obtained by the method described previously. Prior to measurement, cellulose pellets (diameter, 13 mm) were made by grinding and careful homogenization of 35 mg of the material and 100 mg of cellulose to minimize self-absorption and pressing pellets using a laboratory press (Carver, maximum 6 metric tons). Thin films were prepared via drop-casting from a 1 M solution of the materials in MeCN onto Kapton foil and dried at 60 °C for 20 min in air.

Cu K XANES and EXAFS at the Cu K edge scans were recorded for the following samples: complex **1**, crystal and film; complex **2**, crystal, film, and powder; complex **3**, crystal only. The spectra were measured at the SUL-X wiggler beamline of the synchrotron radiation facility ANKA at KIT. A silicon (111) crystal pair with a fixed beam exit was used as monochromator. The X-ray beam is focused to a slit system and collimated with a Kirkpatrick−Baez mirror pair to the sample position. The beam size at sample position was approximately 800 μm × 800 μm. A monochromator stabilizer was used to keep the incoming intensity constant; for this purpose, the monochromator was detuned to 70% maximum intensity. A thin Cu foil (4 μm) as a reference for energy calibration was measured simultaneously with each sample in transmission mode. Irradiation effects on spectral features were investigated by a series of quick scans, and the total exposure time on each sample spot was set such that irradiation effects in the spectra are negligible. The final scans were repeated on different sample positions to improve the signal-to-noise ratio. Up to three scans were accumulated for each spectrum. The energy step width in the XANES region was 0.4 eV. In the EXAFS region, the measuring time per k step (width, 0.05 Å^{-1}) was modulated with the square root of k to improve the signal-to-noise ratio with increasing energy. All measurements were performed in air and at room temperature. For normalization, the intensity of the primary beam was measured by an ionization chamber. Spectra were measured in transmission mode for pellet samples and fluorescence mode for film samples. Transmission intensities were acquired with ionization chambers (Oxford IC10 and ADC) set to 15−40% absorption for the three chambers. Fluorescence intensities were collected with a seven element Si(Li) solid-state detector (SGX Sensortech, formerly Gresham) with the energy window set to the Cu Kα fluorescence emission lines. Signals were dead-time-corrected, glitches were removed, and signals were summed for all channels and divided by the input intensity. The energy scale was calibrated by assigning the first inflection point of the Cu foil spectrum to 8980.3 eV.

All XAS data were analyzed using the program IFEFFIT version 1.2.11.[92] The XANES data were processed using the AUTOBK algorithm of ATHENA.[93] A line was regressed to the data in the pre-edge range, and a quadratic polynomial was used as the post-edge line. The EXAFS analysis was performed by the ARTEMIS[93] software. The scattering amplitudes and phases were calculated with the ab initio FEFF 8.4[94,95] code. The Cu−N, Cu−P, Cu−I, and Cu−Cu single scattering paths were generated using interatomic distances derived from structure obtained from the single-crystal X-ray diffraction analysis of the corresponding crystalline samples. A k range of k = 2.3−12.2 Å^{-1}/k = 2.3−11.2 Å^{-1} was Fourier transformed (FT) for

dx.doi.org/10.1021/ic500135m | Inorg. Chem. 2014, 53, 7837−7847

crystalline and powder/film samples. A shorter k range was chosen for film samples due to a higher signal-to-noise ratio. Hanning windows with $dk = 2$ were used. Fitting was performed in R space for 1.00−3.40 Å with multiple k weights of 1, 2, and 3. The amplitude reduction factor $S_0^2 = 0.9$, which accounts for multielectronic excitations, is obtained from a fit of an EXAFS spectrum of a metallic Cu foil measured in the same experimental conditions. S_0^2 is fixed to 0.9 for all fits. The assumption that S_0^2 is not dependent on the chemical properties of surrounding absorber atoms is a widely used approximation.[81,96−98] Note that $S_0^2 = 0.95$ is calculated with FEFF8.4 for the complexes studied here, but we maintained $S_0^2 = 0.9$ as an appropriate approximation to follow the customary approach. The threshold energy E_0 was allowed to vary for each fit but was constrained to the same value for all paths in a given fit. In a first step, the Cu−N, Cu−P, and Cu−I paths were used to fit the first shell. The coordination numbers (N(N), N(P), and N(I)), change in bond distance R (ΔR), and the mean-squared thermal and static atomic displacement (the Debye−Waller factor σ^2) were varied for all paths. In a second step, the second shell was included in the fit. The Cu−Cu path was added to the model and the coordination numbers and changes in distance were consecutively varied, such that the number of variables was kept to half or less the number of independent data points. The N(I) coordination number was varied, whereas the N(Cu) was restrained (N(I) + N(Cu) = 3) during the fit. Independent variables were added by assigning one parameter for each ΔR and σ^2 to phosphorus/nitrogen, iodine, and copper. Best fits were chosen based on lowest values for χ_ν^2 and the Rfactor.

■ ASSOCIATED CONTENT

Supporting Information

Text describing the fitting of the emission decay parameters and accompanying references, tables listing fitting results of emission decay times for neat film samples and EXAFS results for crystalline, amorphous powder, and film samples, and figures showing photoluminescence spectra of the neat film samples, XANES spectra, and EXAFS fitting results of complex **2**. This material is available free of charge via the Internet at http://pubs.acs.org.

■ AUTHOR INFORMATION

Corresponding Authors

*(S.B.) Fax: +49 721 608 48581. Tel.: +49 721 608 42903. E-mail: braese@kit.edu

*(T.B.) Tel.: +49 721 608 29006. E-mail: baumann@cynora.com.

*(L.W.) E-mail: lothar.weinhardt@kit.edu.

Present Addresses

[†]Institute of Organic Chemistry, Karlsruhe Institute of Technology (KIT), Fritz-Haber-Weg 6, 76131 Karlsruhe, Germany.

[‡]Institute for Photon Science and Synchrotron Radiation (IPS), Karlsruhe Institute of Technology (KIT), Hermann-v.-Helmholtz-Platz 1, 76344 Eggenstein-Leopoldshafen, Germany.

[§]cynora GmbH, Werner-von-Siemens-Straße 2-6, Building 5110, 76646 Bruchsal, Germany.

[∥]Institute of Biological Interfaces 2, KIT, Hermann-v.-Helmholtz-Platz 1, 76344 Eggenstein-Leopoldshafen, Germany.

[⊥]ANKA Synchrotron Radiation Facility, KIT, Hermann-v.-Helmholtz-Platz 1, 76344 Eggenstein-Leopoldshafen, Germany.

[#]Institute for Nuclear Waste Disposal, KIT, Hermann-v.-Helmholtz-Platz 1, 76344 Eggenstein-Leopoldshafen, Germany.

[∇]Department of Chemistry, University of Nevada, Las Vegas (UNLV), 4505 Maryland Pkwy., Las Vegas, NV 89154-4003, USA.

[○]Institute for Chemical Technology and Polymer Chemistry (ITCP), KIT, Engesserstrasse 18/20, 76128 Karlsruhe, Germany.

[◆]Institute of Toxicology and Genetics, KIT, Hermann-v.-Helmholtz-Platz 1, D-76344 Eggenstein-Leopoldshafen, Germany.

Author Contributions

[¶]D.V. and M.W. contributed equally to this manuscript.

Notes

The authors declare no competing financial interest.

■ ACKNOWLEDGMENTS

This work was supported by the Verband der Chemischen Industrie (VCI), Deutsche Telekom Stiftung, the Programmes "BioInterfaces" (BIF) and "Research with Photons, Neutrons, and Ions" (PNI) of the German Helmholtz-Association, and the Deutsche Forschungsgemeinschaft (DFG) via the transregional collaborative research centre SFB/TRR 88 "3MET". We acknowledge ANKA for granting beam time in the proposal MAT-023.

■ REFERENCES

(1) Gan, X.; Fu, W.-F.; Lin, Y.-Y.; Yuan, M.; Che, C.-M.; Chi, S.-M.; Li, H.-F. J.; Chen, J.-H.; Chen, Y.; Zhou, Z.-Y. *Polyhedron* **2008**, *27*, 2202.

(2) Hashimoto, M.; Igawa, S.; Yashima, M.; Kawata, I.; Hoshino, M.; Osawa, M. *J. Am. Chem. Soc.* **2011**, *133*, 10348.

(3) Ogura, T.; Fernando, Q. *Inorg. Chem.* **1973**, *12*, 2611.

(4) Hsu, C.-W.; Lin, C.-C.; Chung, M.-W.; Chi, Y.; Lee, G.-H.; Chou, P.-T.; Chang, C.-H.; Chen, P.-Y. *J. Am. Chem. Soc.* **2011**, *133*, 12085.

(5) Armaroli, N.; Accorsi, G.; Cardinali, F.; Lostorti, A. *Top. Curr. Chem.* **2007**, *280*, 69.

(6) Araki, H.; Tsuge, K.; Sasaki, Y.; Ishizaka, S.; Kitamura, N. *Inorg. Chem.* **2005**, *44*, 9667.

(7) Araki, H.; Tsuge, K.; Sasaki, Y.; Ishizaka, S.; Kitamura, N. *Inorg. Chem.* **2007**, *46*, 10032.

(8) Volz, D.; Nieger, M.; Friedrichs, J.; Baumann, T.; Bräse, S. *Langmuir* **2013**, *29*, 3034.

(9) Liu, Z.; Qayyum, M. F.; Wu, C.; Whited, M. T.; Djurovich, P. I.; Hodgson, K. O.; Hedman, B.; Solomon, E. I.; Thompson, M. E. *J. Am. Chem. Soc.* **2011**, *133*, 3700.

(10) Deaton, J. C.; Switalski, S. C.; Kondakov, D. Y.; Young, R. H.; Pawlik, T. D.; Giesen, D. J.; Harkins, S. B.; Miller, A. J. M.; Mickenberg, S. F.; Peters, J. C. *J. Am. Chem. Soc.* **2010**, *132*, 9499.

(11) Volz, D.; Baumann, T.; Flügge, H.; Mydlak, M.; Grab, T.; Bächle, M.; Barner-Kowollik, C.; Bräse, S. *J. Mater. Chem.* **2012**, *22*, 20786.

(12) Zhang, Q.; Komino, T.; Huang, S.; Matsunami, S.; Goushi, K.; Adachi, C. *Adv. Funct. Mater.* **2012**, *22*, 2327.

(13) Wada, A.; Zhang, Q.; Yasuda, T.; Takasu, I.; Enomoto, S.; Adachi, C. *Chem. Commun. (Cambridge, U. K.)* **2012**, *48*, 5340.

(14) Costa, R. D.; Tordera, D.; Ortí, E.; Bolink, H. J.; Schönle, J.; Graber, S.; Housecroft, C. E.; Constable, E. C.; Zampese, J. a. *J. Mater. Chem.* **2011**, *21*, 16108.

(15) Liu, X.; Sun, W.; Zou, L.; Xie, Z.; Li, X.; Lu, C.; Wang, L.; Cheng, Y. *Dalton Trans.* **2012**, *41*, 1312.

(16) Beltramini, M.; Dimuro, P.; Rocco, G. P.; Salvato, B. *Arch. Biochem. Biophys.* **1994**, *313*, 318.

(17) McMillin, D. R.; Hudson, B. P.; Liu, F.; Sou, J.; Berger, D. J.; Meadows, K. A. In *Photosensitive Metal—Organic Systems*; Kutal, C., Serpone, N., Eds.; American Chemical Society: Washington, DC, USA, 1993; pp 211−231.

(18) Zink, D. M.; Bächle, M.; Baumann, T.; Nieger, M.; Kühn, M.; Wang, C.; Klopper, W.; Monkowius, U.; Hofbeck, T.; Yersin, H.; Bräse, S. *Inorg. Chem.* **2013**, *52*, 2292.

(19) Volz, D.; Zink, D. M.; Bocksrocker, T.; Friedrichs, J.; Nieger, M.; Baumann, T.; Lemmer, U.; Bräse, S. *Chem. Mater.* **2013**, *25*, 3414.
(20) Méhes, G.; Nomura, H.; Zhang, Q.; Nakagawa, T.; Adachi, C. *Angew. Chem., Int. Ed.* **2012**, *51*, 11311.
(21) Tanaka, H.; Shizu, K.; Miyazaki, H.; Adachi, C. *Chem. Commun. (Cambridge, U. K.)* **2012**, *48*, 11392.
(22) Czerwieniec, R.; Yu, J.; Yersin, H. *Inorg. Chem.* **2011**, *50*, 8293.
(23) Yersin, H.; Rausch, A. F.; Czerwieniec, R.; Hofbeck, T.; Fischer, T. *Coord. Chem. Rev.* **2011**, *255*, 2622.
(24) Volz, D.; Bergmann, L.; Zink, D. M.; Baumann, T.; Bräse, S. *SPIE Newsroom* **2013**.
(25) Baldo, M.; Thompson, M.; Forrest, S. *Nature* **2000**, *403*, 750.
(26) Czerwieniec, R.; Kowalski, K.; Yersin, H. *Dalton Trans.* **2013**, 21.
(27) Gather, M. C.; Köhnen, A.; Meerholz, K. *Adv. Mater.* **2011**, *23*, 233.
(28) Köhnen, A.; Riegel, N.; Kremer, J. H.-W. M.; Lademann, H.; Müller, D. C.; Meerholz, K. *Adv. Mater.* **2009**, *21*, 879.
(29) Wada, A.; Zhang, Q.; Yasuda, T.; Takasu, I.; Enomoto, S.; Adachi, C. *Chem. Commun. (Cambridge, U. K.)* **2012**, *48*, 5340.
(30) Liu, Z.; Djurovich, P. I.; Whited, M. T.; Thompson, M. E. *Inorg. Chem.* **2012**, *51*, 230.
(31) Zhang, L.; Li, B.; Su, Z. *Langmuir* **2009**, *25*, 2068.
(32) Tsuboyama, A.; Iwawaki, H.; Furugori, M.; Mukaide, T.; Kamatani, J.; Igawa, S.; Moriyama, T.; Miura, S.; Takiguchi, T.; Okada, S.; Hoshino, M.; Ueno, K. *J. Am. Chem. Soc.* **2003**, *125*, 12971.
(33) Rausch, A. F.; Thompson, M. E.; Yersin, H. *Inorg. Chem.* **2009**, *48*, 1928.
(34) Itokazu, M. K.; Polo, A. S.; Iha, N. Y. M. *J. Photochem. Photobiol., A* **2003**, *160*, 27.
(35) Wrighton, M.; Morse, D. L. *J. Am. Chem. Soc.* **1974**, *96*, 998.
(36) Lees, A. *Coord. Chem. Rev.* **1998**, *177*, 3.
(37) Danielson, E.; Lumpkin, R. S.; Meyer, T. J. *J. Phys. Chem.* **1987**, *91*, 1305.
(38) Thompson, D. W.; Fleming, C. N.; Myron, B. D.; Meyer, T. J. *J. Phys. Chem. B* **2007**, *111*, 6930.
(39) Von Arx, M. E.; Burattini, E.; Hauser, A.; van Pieterson, L.; Pellaux, R.; Decurtins, S. *J. Phys. Chem. A* **2000**, *104*, 883.
(40) Tamayo, A. B.; Garon, S.; Sajoto, T.; Djurovich, P. I.; Tsyba, I. M.; Bau, R.; Thompson, M. E. *Inorg. Chem.* **2005**, *44*, 8723.
(41) Ahuja, R.; Nethaji, M.; Samuelson, A. G. *J. Organomet. Chem.* **2009**, *694*, 1144.
(42) Zink, D. M.; Grab, T.; Baumann, T.; Nieger, M.; Barnes, E. C.; Klopper, W.; Bräse, S. *Organometallics* **2011**, *30*, 3275.
(43) Felder, D.; Nierengarten, J. F.; Barigelletti, F.; Ventura, B.; Armaroli, N. *J. Am. Chem. Soc.* **2001**, *123*, 6291.
(44) Moudam, O.; Kaeser, A.; Delavaux-Nicot, B.; Duhayon, C.; Holler, M.; Accorsi, G.; Armaroli, N.; Séguy, I.; Navarro, J.; Destruel, P.; Nierengarten, J.-F.; Se, I. *Chem. Commun. (Cambridge, U. K.)* **2007**, *3092*, 3077.
(45) Zink, D. M.; Volz, D.; Baumann, T.; Mydlak, M.; Flügge, H.; Friedrichs, J.; Nieger, M.; Bräse, S. *Chem. Mater.* **2013**, *25*, 4471.
(46) Crespo, O.; Gimeno, M. C.; Laguna, A.; Larraz, C. *Z. Naturforsch.* **2009**, *64b*, 1525.
(47) Chen, K.; Strasser, C. E.; Schmitt, J. C.; Shearer, J.; Catalano, V. J. *Inorg. Chem.* **2012**, *51*, 1207.
(48) Mayerle, J. J.; Lippard, S. J. *Inorg. Chem.* **1972**, *11*, 753.
(49) Fife, D. J.; Moore, W. M.; Morse, K. W. *Inorg. Chem.* **1984**, *23*, 1684.
(50) Bommer, J. C.; Morse, K. W. *Inorg. Chem.* **1983**, *596*, 592.
(51) Ganesamoorthy, C.; Balakrishna, M. S.; Mague, J. T. *Inorg. Chem.* **2009**, *48*, 3768.
(52) Ganesamoorthy, C.; Balakrishna, M. S.; George, P. P.; Mague, J. T. *Inorg. Chem.* **2007**, *46*, 848.
(53) Leiva, A. M.; Rivera, L.; Loeb, B. *Polyhedron* **1991**, *I*, 347.
(54) Schmittel, M.; Ganz, A. *Chem. Commun. (Cambridge, U. K.)* **1997**, 999.
(55) Pellegrin, Y.; Sandroni, M.; Blart, E.; Planchat, A.; Evain, M.; Bera, N. C.; Kayanuma, M.; Sliwa, M.; Rebarz, M.; Poizat, O.; Daniel, C.; Odobel, F. *Inorg. Chem.* **2011**, *50*, 11309.
(56) Kaeser, A.; Mohankumar, M.; Mohanraj, J.; Monti, F.; Holler, M.; Cid, J.-J.; Moudam, O.; Nierengarten, I.; Karmazin-Brelot, L.; Duhayon, C.; Delavaux-Nicot, B.; Armaroli, N.; Nierengarten, J.-F. *Inorg. Chem.* **2013**, DOI: 10.1021/ic4020042.
(57) Cid, J.-J.; Mohanraj, J.; Mohankumar, M.; Holler, M.; Accorsi, G.; Brelot, L.; Nierengarten, I.; Moudam, O.; Kaeser, A.; Delavaux-Nicot, B.; Armaroli, N.; Nierengarten, J.-F. *Chem. Commun. (Cambridge, U. K.)* **2013**, *49*, 859.
(58) Maekawa, M.; Munakata, M.; Kitagawa, S.; Yonezawa, T. *Bull. Chem. Soc. Jpn.* **1991**, *64*, 2286.
(59) Li, Y.-J.; Deng, Z.-Y.; Xu, X.-F.; Wu, H.-B.; Cao, Z.-X.; Wang, Q.-M. *Chem. Commun. (Cambridge, U. K.)* **2011**, *47*, 9179.
(60) Lastra, E.; Gamasa, M. P.; Gimeno, J.; Lanfranchi, M.; Tiripicchio, A. *Dalton Trans.* **1989**, 1499.
(61) Field, J. S.; Haines, R. J.; Warwick, B.; Zulu, M. M. *Polyhedron* **1996**, *15*, 3741.
(62) Starosta, R.; Puchalska, M.; Cybińska, J.; Barys, M.; Mudring, A. V. *Dalton Trans.* **2011**, *40*, 2459.
(63) Maini, L.; Braga, D.; Mazzeo, P. P.; Ventura, B. *Dalton Trans.* **2012**, *41*, 531.
(64) Effendy; Di Nicola, C.; Fianchini, M.; Pettinari, C.; Skelton, B. W.; Somers, N.; White, A. H. *Inorg. Chim. Acta* **2005**, *358*, 763.
(65) Zink, D. M.; Volz, D.; Baumann, T.; Mydlak, M.; Flügge, H.; Friedrichs, J.; Nieger, M.; Bräse, S. *Chem. Mater.* **2013**, *25*, 4471.
(66) O'Connor, D. V.; Ware, W. R.; Andre, J. C. *J. Phys. Chem.* **1979**, *83*, 1333.
(67) Ford, P. C.; Cariati, E.; Bourassa, J. *Chem. Rev.* **1999**, *99*, 3625.
(68) Walther, T. H.; Grage, S. L.; Roth, N.; Ulrich, A. S. *J. Am. Chem. Soc.* **2010**, *132*, 15945.
(69) Hanna, J. V.; Smith, M. E.; Stuart, S. N.; Healy, P. C. *J. Phys. Chem.* **1992**, *96*, 7560.
(70) Olivieri, A. *J. Am. Chem. Soc.* **1992**, *114*, 5758.
(71) Tang, J. A.; Ellis, B. D.; Warren, T. H.; Hanna, J. V.; Macdonald, C. L. B.; Schurko, R. W. *J. Am. Chem. Soc.* **2007**, *129*, 13049.
(72) King, R. W.; Huttemann, T. J.; Verkade, J. G. *Chem. Commun. (Cambridge, U. K.)* **1965**, 561a.
(73) Floriano, P. N.; Schoonmaker, J. M.; Poliakoff, E. D.; McCarley, R. L. *J. Am. Chem. Soc.* **2001**, *123*, 10545.
(74) Solomon, E. I.; Szilagyi, R. K.; DeBeer George, S.; Basumallick, L. *Chem. Rev.* **2004**, *104*, 419.
(75) Kuang, S.-M.; Cuttell, D. G.; McMillin, D. R.; Fanwick, P. E.; Walton, R. A. *Inorg. Chem.* **2002**, *41*, 3313.
(76) Mara, M. W.; Jackson, N. E.; Huang, J.; Stickrath, A. B.; Zhang, X.; Gothard, N. A.; Ratner, M. A.; Chen, L. X. *J. Phys. Chem. B* **2013**, *117*, 1921.
(77) Smolentsev, G.; Sukharina, G.; Soldatov, A. V.; Chen, L. X. *Nucl. Instrum. Methods Phys. Res.* **2009**, *603*, 122.
(78) Penfold, T. J.; Karlsson, S.; Capano, G.; Lima, F. A.; Rittmann, J.; Reinhard, M.; Rittmann-Frank, H.; Bräm, O.; Baranoff, E.; Abela, R.; Tavernelli, I.; Rothlisberger, U.; Milne, C. J.; Chergui, M. *J. Phys. Chem. A* **2013**, DOI: 10.1021/jp403751m.
(79) McMillin, D. R.; Kirchhoff, J. R.; Goodwin, K. V. *Coord. Chem. Rev.* **1985**, *64*, 83.
(80) Chen, L. X.; Shaw, G. B.; Novozhilova, I.; Liu, T.; Jennings, G.; Attenkofer, K.; Meyer, G. J.; Coppens, P. *J. Am. Chem. Soc.* **2003**, *125*, 7022.
(81) Jeong, E.-S.; Park, J.; Park, J.-G.; Adipranoto, D. S.; Kamiyama, T.; Han, S.-W. *J. Phys.: Condens. Matter* **2011**, *23*, 175402.
(82) Blackburn, N. J.; Strange, R. W.; Reedijk, J.; Volbeda, A.; Farooq, A.; Karlin, K. D.; Zubieta, J. *Inorg. Chem.* **1989**, *28*, 1349.
(83) Kau, L. S.; Spira-Solomon, D. J.; Penner-Hahn, J. E.; Hodgson, K. O.; Solomon, E. I. *J. Am. Chem. Soc.* **1987**, *109*, 6433.
(84) Hahn, J. E.; Scott, R. A.; Hodgson, K. O.; Doniach, S.; Desjardins, S. R.; Solomon, E. I. *Chem. Phys. Lett.* **1982**, *88*, 595.
(85) Pickering, I. J.; George, G. N.; Dameron, C. T.; Kurz, B.; Winge, D. R.; Dance, I. G. *J. Am. Chem. Soc.* **1993**, *115*, 9498.

(86) Catalano, V. J.; Moore, A. L.; Shearer, J.; Kim, J. *Inorg. Chem.* **2009**, *48*, 11362.
(87) Gaur, A.; Shrivastava, B. D.; Srivastava, K.; Prasad, J.; Raghuwanshi, V. S. *J. Chem. Phys.* **2013**, *139*, 034303.
(88) Cotelesage, J. J. H.; Pushie, M. J.; Grochulski, P.; Pickering, I. J.; George, G. N. *J. Inorg. Biochem.* **2012**, *115*, 127.
(89) Pearson, K. *Philos. Mag.* **1900**, *50*, 157.
(90) Metz, G.; Wu, X. L.; Smith, S. O. *J. Magn. Reson., Ser. A* **1994**, *110*, 219.
(91) Szeverenyi, N. M.; Sullivan, M. J.; Maciel, G. E. *J. Magn. Reson.* **1982**, *47*, 462.
(92) Newville, M. *J. Synchrotron Radiat.* **2001**, *8*, 96.
(93) Ravel, B.; Newville, M. *J. Synchrotron Radiat.* **2005**, *12*, 537.
(94) Moreno, M. S.; Jorissen, K.; Rehr, J. J. *Micron* **2007**, *38*, 1.
(95) Ankudinov, A.; Nesvizhskii, A.; Rehr, J. *Phys. Rev. B* **2003**, *67*, 115120.
(96) Meitzner, G.; Via, G. H.; Lytle, F. W.; Sinfelt, J. H. *J. Chem. Phys.* **1985**, *83*, 353.
(97) Banci, L.; Bertini, I.; Cantini, F.; Ciofi-Baffoni, S.; Gonnelli, L.; Mangani, S. *J. Biol. Chem.* **2004**, *279*, 34833.
(98) Han, S.-W.; Stern, E.; Haskel, D.; Moodenbaugh, A. *Phys. Rev. B* **2002**, *66*, 094101.

dx.doi.org/10.1021/ic500135m | *Inorg. Chem.* 2014, 53, 7837−7847